

Article

Gold-Platinum Core-Shell Nanoparticles with Thiolated Polyaniline and Multi-Walled Carbon Nanotubes for the Simultaneous Voltammetric Determination of Six Drug Molecules

Shaopei Li [†] , Jiayun Zhou [†], Meissam Noroozifar  and Kagan Kerman ^{*} 

Department of Physical and Environmental Sciences, University of Toronto Scarborough, 1265 Military Trail, Toronto, ON M1C 1A4, Canada; shaopei.li@mail.utoronto.ca (S.L.); jiayun.zhou@mail.utoronto.ca (J.Z.); m.noroozifar@utoronto.ca (M.N.)

* Correspondence: kagan.kerman@utoronto.ca

† These authors contributed equally to the work.

Abstract: In this proof-of-concept study, a novel nanocomposite of the thiolated polyaniline (tPANI), multi-walled carbon nanotubes (MWCNTs) and gold–platinum core-shell nanoparticles (Au@Pt) (tPANI-Au@Pt-MWCNT) was synthesized and utilized to modify a glassy carbon electrode (GCE) for simultaneous voltammetric determination of six over-the-counter (OTC) drug molecules: ascorbic acid (AA), levodopa (LD), acetaminophen (AC), diclofenac (DI), acetylsalicylic acid (AS) and caffeine (CA). The nanocomposite (tPANI-Au@Pt-MWCNT) was characterized with transmission electron microscopy (TEM), Fourier-transform infrared spectroscopy (FT-IR), and X-ray photoelectron spectroscopy (XPS). Using the sensor (GCE-tPANI-Au@Pt-MWCNT) in connection with differential pulse voltammetry (DPV), the calibration plots were determined to be linear up to 570.0, 60.0, 60.0, 115.0, 375.0 and 520.0 μM with limit of detection (LOD) of 1.5, 0.25, 0.15, 0.2, 2.0, and 5.0 μM for AA, LD, AC, DI, AS and CA, respectively. The nanocomposite-modified sensor was successfully used for the determination of these redox-active compounds in commercially available OTC products such as energy drinks, cream and tablets with good recovery yields ranging from 95.48 ± 0.53 to $104.1 \pm 1.63\%$. We envisage that the electrochemical sensor provides a promising platform for future applications towards the detection of redox-active drug molecules in pharmaceutical quality control studies and forensic investigations.

Keywords: drug analysis; electrochemical sensor; voltammetry; polyaniline; gold–platinum core-shell nanoparticles; multi-walled carbon nanotubes; over-the-counter drugs



Citation: Li, S.; Zhou, J.; Noroozifar, M.; Kerman, K. Gold-Platinum Core-Shell Nanoparticles with Thiolated Polyaniline and Multi-Walled Carbon Nanotubes for the Simultaneous Voltammetric Determination of Six Drug Molecules. *Chemosensors* **2021**, *9*, 24. <https://doi.org/10.3390/chemosensors9020024>

Academic Editor: Alexander G. Bannov

Received: 9 December 2020

Accepted: 21 January 2021

Published: 28 January 2021

Publisher's Note: MDPI stays neutral with regard to jurisdictional claims in published maps and institutional affiliations.



Copyright: © 2021 by the authors. Licensee MDPI, Basel, Switzerland. This article is an open access article distributed under the terms and conditions of the Creative Commons Attribution (CC BY) license (<https://creativecommons.org/licenses/by/4.0/>).

1. Introduction

Over-the-counter (OTC) drugs are medicines that are sold directly without the requirement of a prescription from a healthcare professional, and are widely used in daily life. Non-steroidal anti-inflammatory drugs (NSAIDs) are marketed as one of the most common OTC pain relievers. NSAIDs control pain and inflammatory conditions by inhibiting two of the closely related cyclooxygenase enzymes, COX-1 and COX-2 [1]. NSAIDs include diclofenac (DI) and acetylsalicylic acid (AS), which are commonly used for the treatment of inflammation, pain, and fever [1]. Ascorbic acid (AA), which is also known as vitamin C, is a vitamin found in various foods and sold as a dietary supplement. AA has been used for pain relief along with the prevention of common cold [2]. Levodopa (LD) is one of the precursors for the biosynthesis of dopamine. Most commonly, LD is used as a dopamine replacement agent for the treatment of Parkinson's disease. It is most effectively used to control bradykinetic symptoms that are apparent in Parkinson's disease [3]. Acetaminophen (AC) is a medication used to treat pain and fever [4]. Caffeine (CA) is a central nervous system stimulant and is widely consumed by people every day, it is also

used to treat tension-type headache. However, overuse of OTC drugs such as AS has been known to suppress prostaglandin production, decreasing the subsequent gastric mucosa layer, reducing gastric acid neutralization that causes stomach ulcers, stomach bleeding and many other intestinal disorders [5]. Whereas overdosing on DI can lead to adverse skin irritation and even in some severe cases respiratory irritations [5]. Thus, it is of a great interest to develop a sensor platform that allows the detection and analysis of the OTC drug molecules.

Several studies on the detection of OTC drugs have been reported using the electrochemical sensors. Sun et al. [6] described a graphene-based electrochemical sensor to detect CA. A novel nanocomposite of Au nanoparticles and multi-walled carbon nanotubes (MWCNTs) was synthesized to provide a sensitive detection of DI [6]. Daneshinejad et al. [7] modified a glassy carbon electrode (GCE) with a thin film of poly(solochrome black T) and this sensor provided a sensitive and selective voltammetric simultaneous determination of dopamine and AC. Wearable electrochemical sensors have recently been utilized to determine patient-specific dose regulation and pharmacokinetics of drug molecules as well as supporting the law enforcement agents with on-site forensic analyses to detect the drugs of abuse [8]. In addition, a GCE modified with Au nanoparticles was developed to detect AA [9]. Moreover, Wudarska et al. [10] utilized a platinum electrode to study the electrochemical behavior of AS. With increasing attention drawn to the convenience of the use of screen-printed electrodes (SPEs), recent literature reported several approaches towards the use of SCEs as the base construct of the novel drug sensor. Previously, Bergamini et al. [11] have reported a gold screen-printed electrode coupled into a microflow cell system to achieve the detection of LD. Later, another group has reported the use of carbon SPEs modified with carbon nanofibers as a new sensor for the detection of AC and ibuprofen demonstrating the application of novel nanocomposites [12]. However, to the best of our knowledge, there is no study that reported a nanocomposite-based electrochemical sensor capable of detecting all six OTC drug molecules such as AA, LD, AC, DI, AS and CA simultaneously using voltammetry.

Recently, the composite structures of conducting polymers with MWCNTs have been widely studied due to ease of preparation and the enhanced electrochemical properties. The MWCNTs are well known for their high tensile strength of most outer layer ranging from 11 to 63 gigaPascals [13]. This high strength is due to its unique structural properties. The MWCNTs consist of multiple rolled layers of graphene [14]. In the graphite layer, the carbon atoms are packed into a benzene-ring structure [15]. Each carbon atom in the graphite layer is covalently bonded to the other surrounding carbon atoms using sp² hybridization and create the structure of a carbon film [16]. The strength of the sp² carbon-carbon bonds provides MWCNTs with high tensile strength [17,18]. As the thin carbon films exhibit a strong ambipolar electric field effect with high electrical conductivity, MWCNTs have become a widely used material for electrochemical sensor fabrication [15,19]. In the literature, MWCNTs were used as the electrode nanocomposite to detect NSAIDs such as AC and DI [6,20]. Polyaniline (PANI) was chosen as the conductive polymer in this study due to its facile preparation and high conductivity. The thiolated PANI (tPANI) contains functional groups such as -SH at its para position, such as 4-aminothiophenol that can be substituted to allow for metal nanoparticles. Secondly, once polymerized, PANI is highly compatible with other carbon-nanomaterials such as MWCNTs. Several studies that combined PANI with MWCNTs achieved significant improvement at lowering the limit of detection (LOD) when detecting ammonia [21,22]. Finally, Au and Pt nanoparticles also have a large surface area, high conductivity and excellent electrocatalytic characteristics that are highly suitable to enhance the sensitivity and the detection limit in an electrochemical sensor construct [23–26]. One of the major challenges in chemical sensors is the task to detect multiple analytes simultaneously that are often found in one sample without having to employ sophisticated separation techniques. A single type of nanocomposite, though it can increase the performance of the sensor, is often limited to the detection of two or three compounds. Thus, the use of hybrid materials has been widely explored for

simultaneous determination of multiple analytes. Hrapovic et al. [26] previously reported a composite of Pt nanoparticles and MWCNTs composite to-wards the detection of glucose. Their reported system was able to reach a remarkable LOD of 0.5 μM in 3 s. This was attributed to the synergistic effect of the high conductance of Pt nanoparticles and the high surface-area-to-volume ratio of the MWCNTs. Additionally, an increase in the electrocatalytic performance was observed for systems combining PANI with MWCNTs. A carbon paste electrode modified with PANI/MWCNTs was reported as a non-enzymatic sensor for cholesterol [27]. Furthermore, our group has reported several nanocomposite-modified chemical sensors, and have demonstrated that the synergistic effect of different materials can result in a significant enhancement in sensitivity, stability, and selectivity towards the target analyte [28–30]. Thus, in this study, the synergistic effect between PANI, MWCNTs, and core-shell nanoparticles was exploited for the fabrication of a novel nanocomposite.

In this study, the fabrication of MWCNTs enveloped by PANI (doped with the thiolated aniline to synthesize tPANI) were decorated with gold–platinum (Au@Pt) core-shell nanoparticles to synthesize a novel nanocomposite, tPANI-MWCNT-Au@Pt, for the simultaneous voltammetric detection of redox-active drug molecules, AA, LD, AC, DI, AS and CA, in a single measurement. To the best of our knowledge, the voltammetric detection of these six drug molecules in a single measurement has been achieved here in this report for the first time. GCE modified with tPANI-MWCNT-Au@Pt (GCE-tPANI-MWCNT-Au@Pt) was further challenged with stability, reproducibility, and recovery tests in commercially available OTC products. The results demonstrated that the sensor was stable, reproducible with excellent sensitivity and a wide dynamic range indicating the future applications of the sensor towards the detection of redox-active drug molecules in quality control and forensic toxicity assays.

2. Materials and Methods

2.1. General Materials

Chloroauric acid (HAuCl_4), chloroplatinic acid (H_2PtCl_6) 4-aminothiophenol, aniline hydrochloride, MWCNTs, AA, LD, AC, DI, AS, and CA were obtained from Sigma-Aldrich Company (Oakville, ON, Canada) and all chemicals were used as received. The electrolyte and buffer solutions with final concentration 0.5 M at pH 2.0–8.0 were prepared using phosphoric acid and NaOH. All solutions were prepared using Milli-Q water (18.2 $\text{M}\Omega\text{ cm}$) obtained from a Cascada LS water purification system (Pall Co., Mississauga, ON, Canada).

2.2. Instrumentation

A Hitachi H7500 Transmission Electron Microscope (Hitachi, Tokyo, Japan). Fourier transform-infrared spectroscopy (FT-IR) spectra were recorded on a Bruker Alpha FT-IR with a Digilab FTS 4000 fitted with an attenuated total reflectance (ATR) (Bruker, Billerica, MA, USA). Angle-resolved X-ray photoelectron spectroscopy (XPS) was performed with a Theta-probe Thermo-Fisher Scientific Instrument (East Grinstead, UK) with a monochromatic Al K α source with a photo energy 1486.6 eV. The accumulated angle was 90° with a 20 eV pass energy at the analyzer at a 10–8 mbar vacuum chamber. The analysis area was 500 μm^2 . An Autolab PGSTAT 128N supported by NOVA™ 2.1 software (Metrohm, Utrecht, The Netherlands) was used for all electrochemical studies. A Metrohm electrochemical cell including a platinum wire and a silver/silver chloride electrode as the counter and reference electrodes, respectively. Glassy carbon electrodes (GCEs, CH Instruments Inc., Austin, TX, USA) were used as the working electrode. All electrochemical impedance spectroscopy (EIS) measurements were performed in 10 mM $[\text{Fe}(\text{CN})_6]^{3-/4-}$ with 0.10 M NaClO_4 at a constant applied potential of 0.20 V (vs. Ag/AgCl) over the frequency range from 100 kHz to 500 mHz with a 10 mV potential amplitude. Differential pulse voltammetry (DPV) was performed in a wide potential window from –0.1 to 1.55 V at a step potential of 5 mV and a modulation amplitude of 0.025 V with a modulation time of 0.05 s as well as an interval time of 0.5 s. For each successive measurement, a freshly prepared

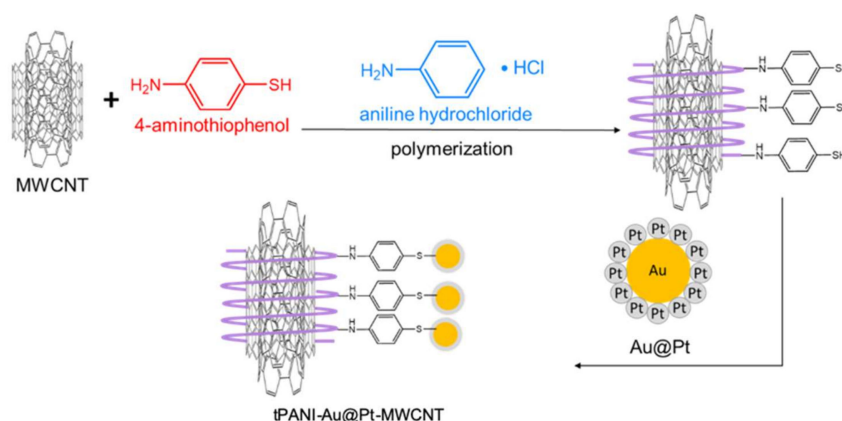
GCE-tPANI-Au@Pt-MWCNT was employed as the working electrode. The electrochemical measurements were repeated in triplicates ($n = 3$), unless otherwise stated.

2.3. Synthesis of Gold-Core Platinum-Shell Nanoparticles (Au@Pt)

The synthesis of Au@Pt was achieved by following a modified version of Frens' method [31,32]. Briefly, an aliquot (10 mg) of HAuCl₄ was dissolved in 100 mL water. The solution was heated to boil and then 1 mL of 0.01 g/mL citrate solution was added. This method was utilized to synthesize the gold nanoparticles with an approximate size of 55 nm in diameter. Then, 30 mL of gold nanoparticles was mixed with 10 mL of 1 mM H₂PtCl₆. This amount of H₂PtCl₆ enabled the synthesis of Pt shell with an approximate thickness of 2.75 nm on gold nanoparticles. Then, the mixture was heated to 80 °C while stirring. An aliquot (5 mL) of 10 mM freshly prepared AA solution was added to the mixture and stirred until the color changed from dark green to brown.

2.4. Preparation of Nanocomposite

Briefly, 100 mg of 4-aminothiophenol and 50 mg of MWCNT were mixed in solid form. Then, 1 mg of aniline and 150 mg of potassium peroxydisulfate were added and dissolved in 5 mL of 1.2 M HCl. The mixture was stirred rapidly for 2 min, and then left at room temperature for 12 h. The color of this mixture turned from light grey to green and finally black during this period. This mixture was collected with filtration and washed with 1 M HCl and then ethanol for three consecutive times. The resulting solid product was dried at room temperature for 12 h and further dried in an oven for 3 h at 70 °C. Then, an aliquot (10 mL) of Au@Pt solution was added to the solution and mixed by shaking. The Au@Pt nanoparticles were adsorbed by the polymer-MWCNT composite. The solution was centrifuged, and the solid nanocomposite was collected and dried at room temperature for 12 h. The synthesis steps of the nanocomposite are briefly illustrated in Scheme 1.



Scheme 1. Schematic illustration depicting the synthesis of thiolated polyaniline multi-walled carbon nanotubes and gold-platinum core-shell nanoparticles (tPANI-Au@Pt-MWCNT) nanocomposite.

2.5. Preparation of Nanocomposite-Modified GCE

GCEs were polished to a mirror finish with alumina powder starting from 1.0 μm , 0.3 μm and 0.05 μm in size for 15 min. The polished GCEs were then sonicated in water for 10 s to remove the remaining alumina powder. The acid-activation was achieved by applying a potential ranging from -1.0 to 1.5 V at a scan rate of 100 mV/s for 30 cycles in 0.5 M H₂SO₄. After gently rinsing with water, the preparation of acid-activated GCEs was completed. The acid-activated GCE surfaces were then modified by drop-casting 20 μL of the freshly prepared nanocomposite dispersed in Nafion™ (1.5% v/v). The modified electrodes (GCE-tPANI-MWCNT-Au@Pt) were allowed to dry for 18 h at room temperature.

2.6. Analyses with Commercial Products

Five of the OTC drugs (AA, AC, DI, AS and CA) were purchased from commercial vendors and dissolved using deionized distilled water. For AA, the energy drink Vitamin Water™ was diluted in a 1:10 dilution with distilled water. For AC, five tablets of pseudoephedrine hydrochloride, which each of the tablet contained 325 mg AC was crushed and powdered first, and then 0.5 g of this powder was dissolved in 50 mL distilled water and then filtered for removing any remaining solids. An amount of 0.0380 g of Voltaren™ cream which contains 23.2 mg/g of DI was dissolved in 50 mL of distilled water to create the stock solution for testing. Then, 5 tablets of Aspirin™ (containing 500 mg AC) was powdered and 0.2 g of the powder was dissolved in 25 mL of distilled water and 70 μL of KOH was added into the solution. Similarly, 5 CA tablets (containing 200 mg CA each) was powdered first and then 0.4 g of this powder was dissolved in 50 mL of distilled water and 600 μL of KOH was added into the solution to prepare the stock solution. All the stock solutions were freshly prepared immediately before the electrochemical measurements.

3. Results and Discussion

3.1. Characterizaion of tPANI-MWCNT-Au@Pt Nanocomposite

To demonstrate the successful synthesis of tPANI-Au@Pt-MWCNT nanocomposite, FT-IR experiments were performed to monitor the stepwise synthetic processes (Figure 1). MWCNTs demonstrated a weak C-C bonding around 3300 cm^{-1} . The monomer, 4-aminothiophenol, demonstrated a primary amine, C-H, and C-SH stretches with an aromatic breathing at $3416, 3301, 3186, 1583\text{--}1487\text{ cm}^{-1}$, respectively. This is consistent with the literature that reported spectra of 4-aminothiophenol [33]. Aniline HCl demonstrated an amine salt stretch at 2797 cm^{-1} , which is common for primary amines when in salt form. In addition, the corresponding CH and aromatic signals were found at $2569, 1575\text{--}1461\text{ cm}^{-1}$, suggesting that unpolymerized aniline was also present. The tPANI-Au@Pt-MWCNT nanocomposite demonstrated a medium peak at $3240, 1298$ and $1575\text{--}1482\text{ cm}^{-1}$, which correlates to the presence of an amide bond, the C-N = bonding between a benzenoid and a quinoid unit and aromatic ring, respectively. This result suggested that the aniline polymerized into PANI and incorporated the MWCNTs forming the final tPANI-Au@Pt-MWCNT nanocomposite.

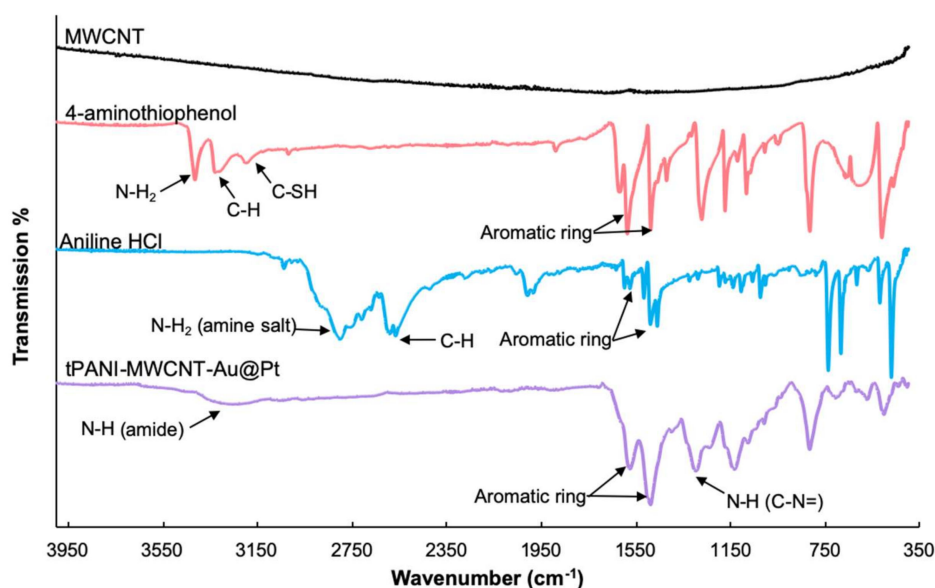


Figure 1. FT-IR spectra of MWCNTs (black), 4-aminothiophenol (red), aniline HCl (blue), and the final nanocomposite tPANI-Au@Pt-MWCNT.

To demonstrate the physical characteristics of the nanocomposite as well as showing that Au@Pt was incorporated into the nanocomposite, the final structure was analyzed

using electron microscopy. Figure 2 displays the TEM of tPANI, Au@Pt, tPANI-MWCNT, tPANI-Au@Pt-MWCNT. Based on Figure 2a,b with different magnifications, the tPANI-SH shows a fiber distribution that randomly oriented with a diameter varying between 65 and 130 nm. The TEM images of Au@Pt are shown in Figure 2d–f with uniform raspberry-like core-shell nanoparticles with a diameter of 33 ± 3 nm. This morphology is in agreement with previous literature where the gold-core nanoparticles coated with platinum exhibited this “fuzzy” raspberry-like structure indicating the formation of the platinum shell [32]. Figure 2g–i show the TEM images of tPANI-MWCNTs with sharp dendritic structures. In TEM images of tPANI-Au@Pt-MWCNT, the dendrites of the tPANI-MWCNT adjoined with each other and trapped MWCNTs and Au@Pt in a cluster. The main reason for this change of physical appearance was attributed to the presence of the Au@Pt nanoparticles. Due to the thiol groups present within the tPANI polymer matrix, Au@Pt nanoparticles might have facilitated the polymer wrapping around the MWCNTs. In addition, since MWCNTs were incorporated into the tPANI, tubular structures were thus observed across the entire cluster. These images suggested that the final tPANI-Au@Pt-MWCNTs nanocomposite was successfully synthesized.

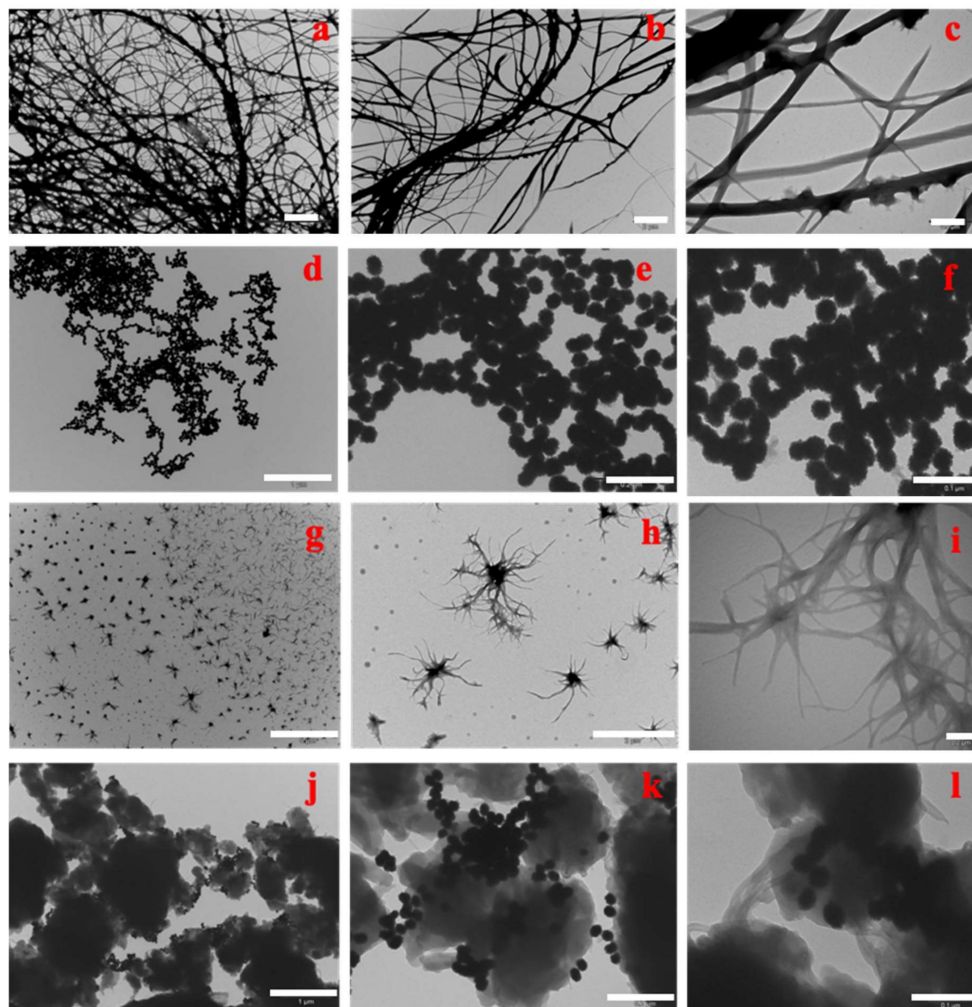


Figure 2. TEM images tPANI with different magnifications with scale bars indicating 5 μm , 2 μm and 0.5 μm in (a), (b) and (c), respectively; Au@Pt core-shell nanoparticles with different magnifications with scale bars indicate 1 μm , 0.2 μm and 0.1 μm in (d), (e) and (f) respectively. tPANI-MWCNT with different magnifications with scale bars indicating 5 μm , 2 μm and 0.2 μm in (g), (h) and (i), respectively; and tPANI-Au@Pt-MWCNT with different magnifications with scale bars indicating 1 μm , 0.2 μm and 0.1 μm in (j), (k) and (l), respectively.

To further characterize the elemental composition of the nanocomposite, XPS was performed and the results are shown in Figure 3 and Figures S1–S3. Figure 3 shows the Au 4f and P 4f for different modified electrodes with tPANI (Figure 3a,b), tPANI-MWCNT (Figure 3c,d), and tPANI-Au@Pt-MWCNT (Figure 3e,f). As expected on the Au 4f and Pt 4f spectra, no observable peaks were found. The XPS of the tPANI is shown in Figure S1. The N1s spectra displayed (Figure S1c) peaks at 399.1 and 401.5 eV correlating to the -N= and -NH- structures, respectively, that are in alignment with the polymerized aniline as reported in a previous study [34]. Sulfur XPS was also performed to observe the -SH group within the tPANI matrix formed by 4-aminothiophenol. As shown in Figure S1d, the S 2p spectrum displayed a 169.7 and 167.8 eV peak corresponding to the -SH group. The high eV value indicated the presence of -SH groups that were not yet bound to metallic elements [34]. For the next step, tPANI-MWCNT (), again, no observable peaks were found on the Au 4f and Pt 4f spectra. C 1s spectra (Figure S2b) demonstrated the incorporation of -SH containing PANI with MWCNT, peaks were found at 289.2, 287.6, 286.4, 285.4, and 283.8 eV correlating to O-COO, -C=O, C-O, sp^3 C-C, and sp^2 C=C, respectively, similar to previously reported values of MWCNTs [35]. In addition, the N 1s spectra (Figure S2c) demonstrated a slight shift in the binding energy, S 2p spectrum shows no change in its profile, this suggested that the tPANI-MWCNT was synthesized successfully. In the final step, the incorporation of Au@Pt produced the final tPANI-Au@Pt-MWCNT nanocomposite. As shown in Figure 3e, the Au 4f spectrum demonstrated peaks at 83.4 and 87.1 eV corresponding to the Au 4f_{7/2} and Au 4f_{5/2} peaks. The Pt 4f spectrum also showed peaks at 71.2 and 74.8 eV, that can be assigned to the Pt 4f_{7/2} and Pt 4f_{5/2} for the Pt⁰. The additional peaks observed at 70.5 and 77.1 eV were attributed to the Pt²⁺ species, and due to the Pt⁰ ratio were higher than the Pt²⁺ peaks, suggesting that Pt⁰ species were dominant as observed in Au@Pt core-shell nanoparticles [32,36]. In addition, Au peaks were lower in intensity compared to the Pt peaks. This is also a characteristic of the Pt shell-gold core nanoparticles that were previously reported [36]. This suggested that the Au@Pt core-shell nanoparticles were obtained. The S 2p spectrum (Figure S3d) also showed a corresponding change, as the 163.2 eV peak indicated that the Au-S bond was formed. N 1s and C 1s spectra (Figure S3b–d) both showed no observable changes, conclusively suggesting that the Au@Pt core-shell nanoparticles were successfully attached to the tPANI wrapping around the MWCNTs creating the nanocomposite PANI-Au@Pt-MWCNT.

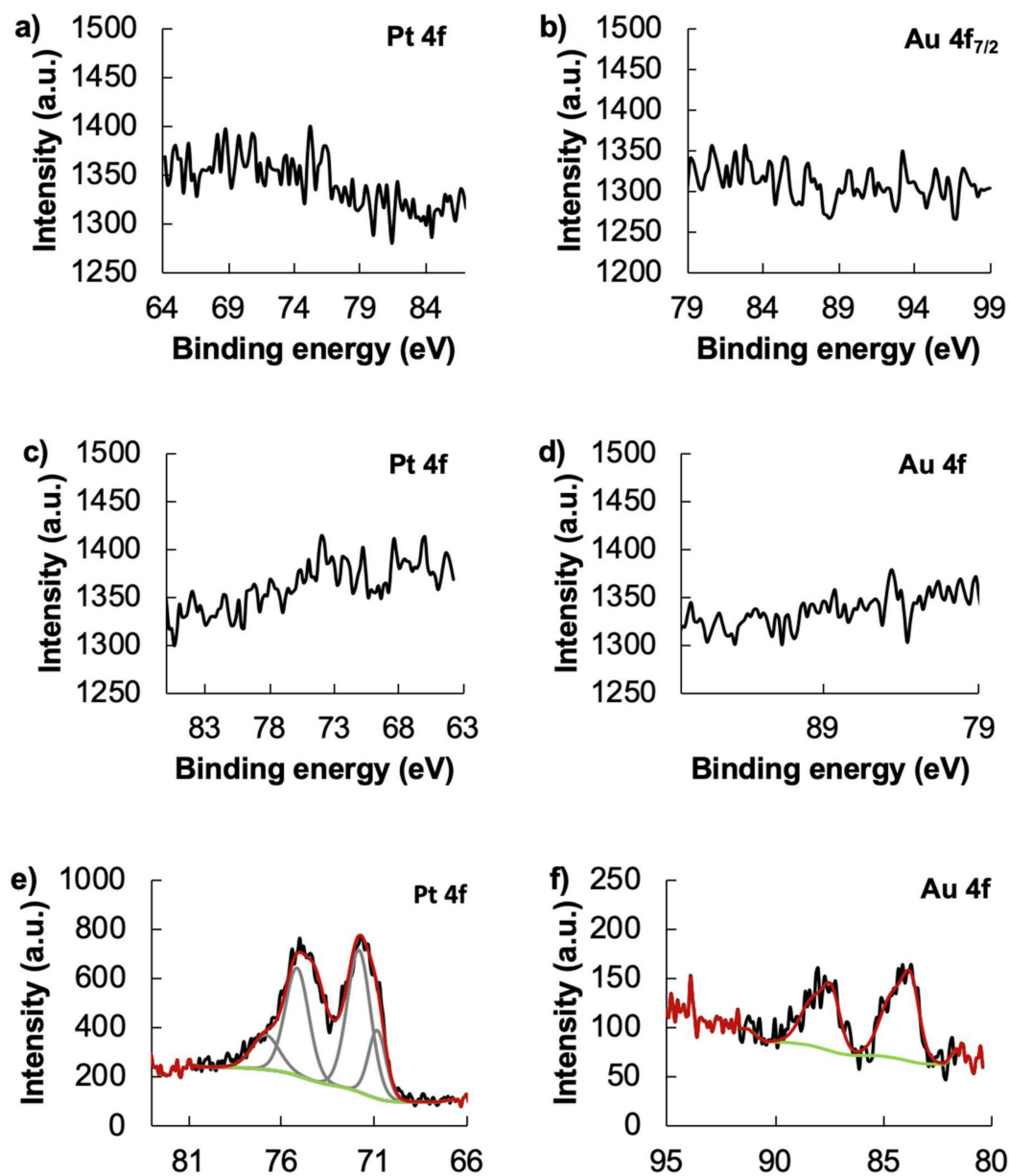


Figure 3. Au and Pt X-ray photoelectric spectra of the characterization of nanocomposite on a glassy carbon electrode (GCE) surface, (a,b) tPANI, (c,d) tPANI-MWCNT, and (e,f) tPANI-Au@Pt-MWCNT.

3.2. Electrochemical Characterization of tPANI-Au@Pt-MWCNT Modified GCE

To analyze the electrochemical activity of the GCE-tPANI-Au@Pt-MWCNT, CV and EIS studies were performed. As shown in Figure 4a, the cyclic voltammograms of GCEs modified with different composite structures were analyzed in 10 mM $\text{Fe}(\text{CN})_6^{3-/4-}$. CV results demonstrated anodic and cathodic peaks at 0.30 V and 0.144 V vs. saturated Ag/AgCl, respectively. When the GCEs were modified with tPANI, a decrease in the current intensity was observed accompanied by the presence of new anodic and cathodic peaks at 0.537 and -0.168 V, which were attributed to the redox signal of tPANI. When MWCNTs were included along with tPANI, an increase in current intensity was observed along with a shift of the anodic and cathodic peak corresponding to $\text{Fe}(\text{CN})_6^{3-/4-}$ to 0.344 V and 0.085 V, respectively. This phenomenon was attributed to the chemical characteristics of sulfonated PANI. The construct incorporated 4-aminothiophenol during the polymer-

ization of PANI, thus, creating gaps between the conductive matrix at the surface and resulting in the decrease in current density. However, when MWCNTs were incorporated, a synergistic effect was observed where the MWCNTs might have bridged the conductive gaps facilitating the electron transfer and increasing the current intensity. In addition, the peaks correlated to the tPANI signal become non-observable. Similarly, current increase also occurred as Au@Pt particles were incorporated into the nanocomposite, but the redox signals of $\text{Fe}(\text{CN})_6^{3-/4-}$ became less obvious in the voltammograms. However, when both MWCNTs and Au@Pt were present in the final composite, a stronger current intensity compared to GCE was observed. Additionally, the $\text{Fe}(\text{CN})_6^{3-/4-}$ was clearly observed at 0.351 V and 0.100 V for the anodic and cathodic peaks, respectively. On the corresponding EIS spectra (Figure 4b), the effect towards surface modification that the nanocomposites imposed was detected.

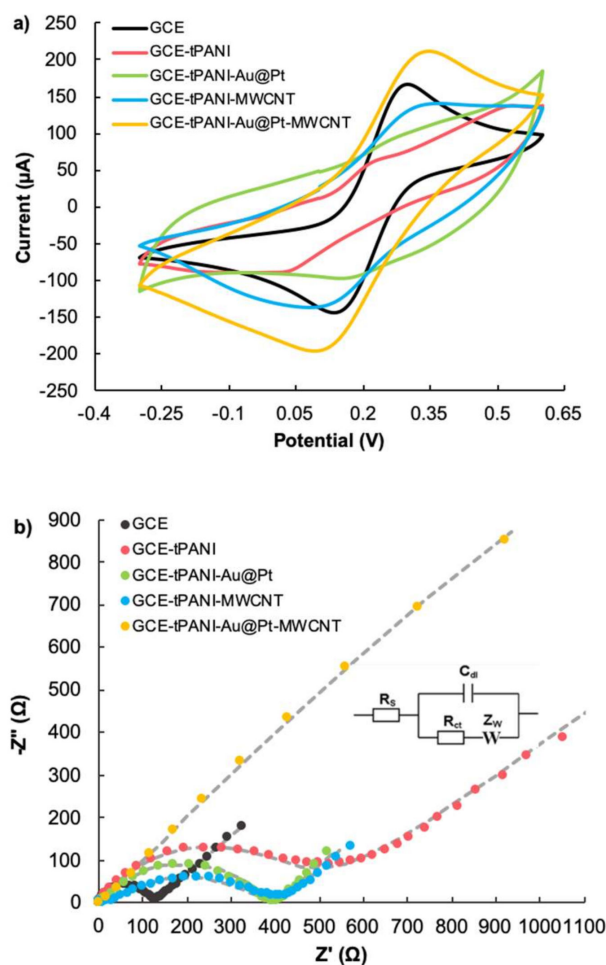


Figure 4. (a) Cyclic voltammograms, and (b) the Nyquist plots of GCEs with various modifications of nanocomposite components. Bare GCEs (black), GCE-tPANI (red), GCE-Au@Pt-tPANI (green), GCE-tPANI-MWCNT (blue), and GCE-tPANI-Au@Pt-MWCNT (yellow) in 10 mM $\text{Fe}(\text{CN})_6^{3-/4-}$ with 0.1 M NaClO_4 as supporting electrolyte. Following EIS studies, the resulting R_{CT} values were extrapolated by fitting the Nyquist plots to a Randles equivalent circuit (shown in **B**, inset).

Blank GCE demonstrated a charge transfer resistance (R_{CT}) of $135.35 \pm 3.496 \Omega$. When GCE was modified with only tPANI, the R_{CT} increased to $569.93 \pm 74.09 \Omega$. When only Au@Pt or only MWCNTs were incorporated along with tPANI, the R_{CT} increased to $396.13 \pm 4.88 \Omega$ and $404 \pm 10.44 \Omega$, respectively. However, when the GCEs were modified with final components as tPANI-Au@Pt-MWCNT, an R_{CT} value was not detected. Firstly, in the sole presence of tPANI, the CV and EIS results suggested that tPANI might

hinder the electron transfer kinetics between the $\text{Fe}(\text{CN})_6^{3-/4-}$ probe and the electrode, suggesting a possible spatial separation within the tPANI polymer network. However, with the incorporation of MWCNTs and Au@Pt, due to their inherent electrocatalytic ability, the nanocomposite might have facilitated the electron transfer process of $\text{Fe}(\text{CN})_6^{3-/4-}$, hence, an increase in current intensity and a decrease in R_{CT} were observed with CV and EIS, respectively. When both Au@Pt and MWCNTs were present, a synergistic catalytic effect along with tPANI was observed. Therefore, these results indicated that the final nanocomposite was able to improve the electrochemical performance of GCE, and a synergistic effect was observed after the modification with MWCNTs and Au@Pt nanoparticles.

3.3. Simultaneous Detection of Six OTC Drug Molecules Using DPV

In order to demonstrate the nanocomposite was effective at enhancing the electrochemical detection of all six OTC drug molecules, a simultaneous comparison study was performed. As shown in Figure 5, GCEs were modified with different nanocomposite structures, and subjected to the detection of AA (150 μM), LD (15 μM), AC (15 μM), DI (15 μM), AS (150 μM), and CA (150 μM) using DPV. Blank GCE displayed low current peaks at 0.24 V, 0.73 V, 0.96 V, and 1.23 V corresponding to the oxidation of AA, DI, AS, and CA, respectively. However, LD and AC were not observable. For tPANI modification, no observable signals were observed except for a large background peak at 0.24 V, which was consistent with CV and EIS results suggesting tPANI alone might not present enough catalytic properties. With the incorporation of Au@Pt with tPANI, the current peaks were detected at 0.52 V and 0.75 V corresponding to the oxidation signals of AC and DI, respectively. In addition, a broad peak between 0.24 V–0.35 V was observed, which could be attributed to the overlapping oxidation signals of AA and LD. For the tPANI-MWCNT, low current peaks at 0.30 V, 0.39 V, and 0.62 V were detected, and were found to be AA, LD and DI but tPANI-MWCNT-modified electrode still was unable to detect all six drug molecules. Finally, using the tPANI-Au@Pt-MWCNT nanocomposite, six well-defined current peaks were detected at 0.30 V, 0.41 V, 0.58 V, 0.76 V, 1.03 V, and 1.37 V for AA, LD, AC, DI, AS, and CA, respectively. All six peaks displayed good separation with clear peak shape. This result suggested that the tPANI-Au@Pt-MWCNT nanocomposite might enhance the overall detection capabilities of the sensor, further supporting that Au@Pt, MWCNT, and tPANI might have a synergistic effect on anodic current responses.

It was necessary to examine the performance of GCE-tPANI-Au@Pt-MWCNT in both individual and mixed solutions of the OTC drug molecules. As shown in Figure 6, DPV peaks were found at approximately 0.29 V, 0.41 V, 0.57 V, 0.79 V, 1.03 V, and 1.38 V, which correspond to the anodic peak of AA (red line), LD (orange line), AC (green line), DI (blue line), AS (grey line) and CA (purple line), respectively. When all six analytes were mixed (black line), the electrochemical oxidation signals correlating to all six OTC drug molecules were detected in a single scan (black line). The low peak recorded at 0.28 V was a characteristic signal for PANI formation as reported in the literature [37].

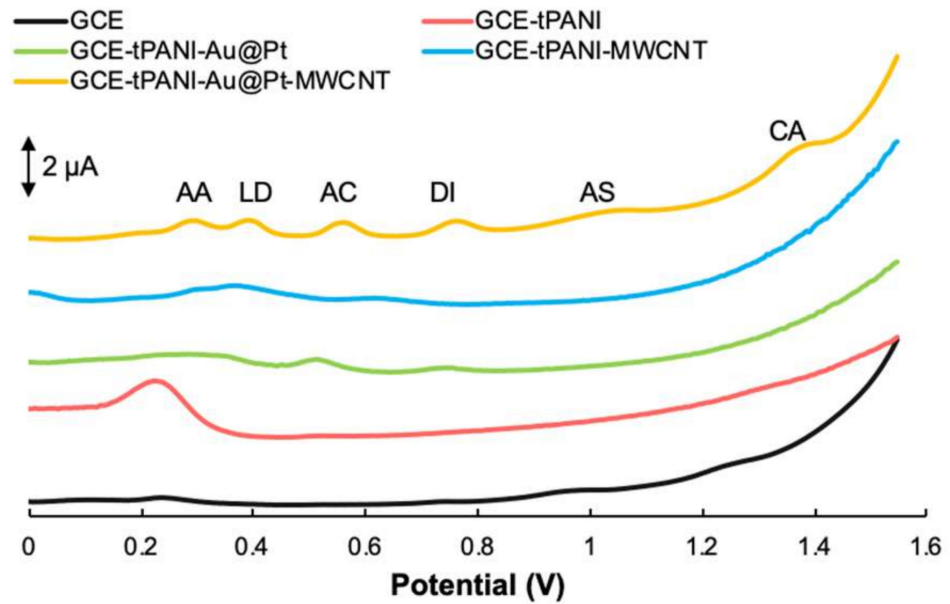


Figure 5. Differential pulse voltammograms for the electrochemical oxidation of ascorbic acid (AA) (150 μM), levodopa (LD) (15 μM), acetaminophen (AC) (15 μM), diclofenac (DI) (15 μM), acetylsalicylic acid (AS) (150 μM), and caffeine (CA) (150 μM) at the blank GCE (black line), tPANI-modified GCE (red line), tPANI-Au@Pt-modified GCE (green line), tPANI-MWCNT-modified GCE (blue line), and tPANI-Au@Pt-MWCNT-modified GCE (yellow line) in 0.5 M PBS (pH 3.0).

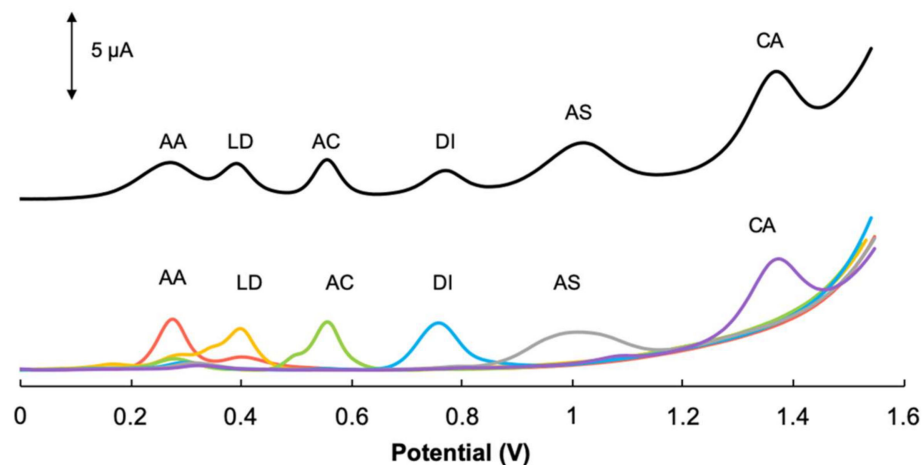
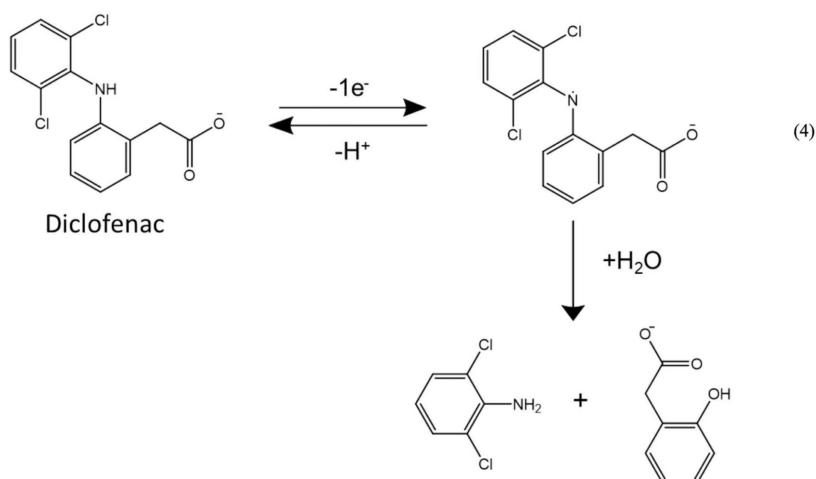
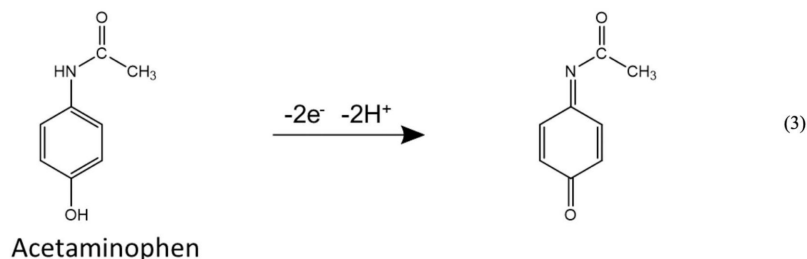
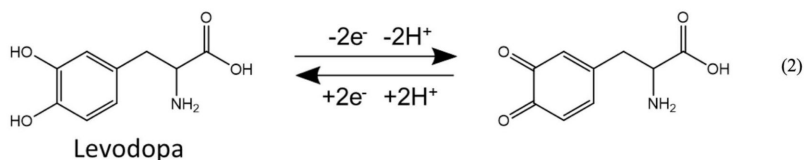
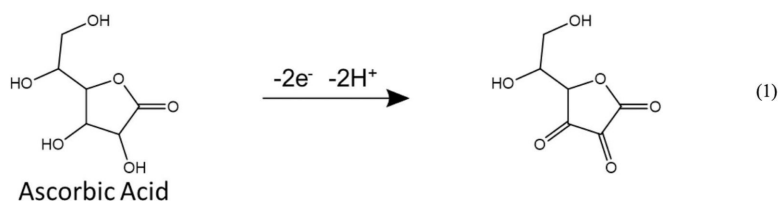


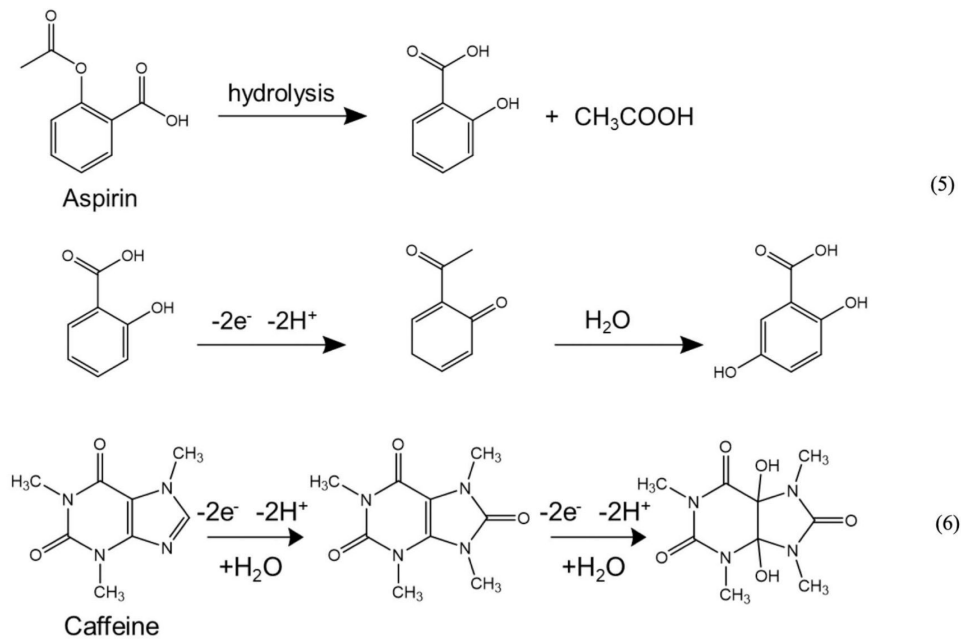
Figure 6. Differential pulse voltammograms of ascorbic acid only (AA, 250 μM , red line), levodopa only (LD, 25 μM , orange line), acetaminophen only (AC, 25 μM , green line), diclofenac only (DI, 25 μM , blue line), acetylsalicylic acid only (AS, 250 μM , grey line) and caffeine only (CA, 245 μM , purple line), and all six over-the-counter (OTC) drug molecules at the same concentrations in one solution (black line) at a GCE-tPANI-Au@Pt-MWCNT in 0.5 M PBS (pH 3.0).

3.4. Effect of pH

To examine the performance of GCE-tPANI-Au@Pt-MWCNT in different pH conditions, the detection of six OTC drug molecules was analyzed using DPV. As shown in Figure S4a, as pH increased, the peak potential of six analytes shifted towards lower potentials. The current peak at pH 3.0 was the most robust, and thus, was determined to be the optimal pH environment for the subsequent detection analysis. Additionally, to further understand the mechanism of the redox processes, the peak potential shift was plotted against the pH (Figure S4b). By fitting the plotted values, a slope was extrapolated for each OTC drug and the results were found to be 0.0534, 0.0554, 0.0504, 0.0393, 0.0307 and 0.001

for AA, LD, AC, DI, AS and CA, respectively. For three of the analytes AA, LD and AC, the slope values were close to the Nernstian value of 0.059 mV/pH for a two-electron and two-proton equivalent exchange mechanism, except for DI, AS and CA. DI and AS might form 3,6-dioxocyclohexa-1,4-dienecarboxylate or 5,6-dioxocyclohexa-1,3-dienecarboxylate and undergo a hydrolysis reaction that involved two-electron and one-proton transfer [38]. For CA, as reported in the previous literature, there is no correlation between the changes in pH and electron transfer during the oxidation reaction [39], which was observed as 0.001 mV/pH calculated from the experimental data. The predicted electrochemical oxidation reactions of AA, LD, AC, DI, AS, and CA are shown in redox process Equations (1)–(6) as follows:





3.5. Calibration Curves

To examine the dependence of peak current signals on the concentration of analytes, calibration curves for six OTC drug molecules were plotted, and the results are shown in Figure 7. The sensor demonstrated a linear response to the addition of analytes at increasing concentrations. The anodic peak current intensity was obtained and plotted against the concentration (Figure S5) and the results are summarized in Table 1. Two-segment linear regression curves were found except for those plotted for AS and CA with a one-segment curve. This effect can be correlated to the decreasing available active surface area. Initially, the concentration of the analyte with the solution was low, the available active surface area on the electrode could rapidly undergo electron exchange reactions. With increasing concentration of the analyte, the available active surface area decreased, which resulted in a less sharp slope. The calibration curves were linear up to 570.0, 60.0, 60.0, 115.0, 375.0 and 520.0 μM with the limit detection ($\text{LOD} = 3S_{\text{bk}}/m$ where S_{bk} and m are standard deviation of blank solution for 10 independent measurements ($n = 10$) and the slope of calibration curves, respectively) 1.5, 0.25, 0.15, 0.2, 2.0 and 5.0 μM for AA, LD, AC, DI, AS and CA, respectively. The figures of merit of the nanocomposite-modified sensor in comparison with the reported ones in literature for the electrochemical determination of AA, LD, AC, DI, AS and CA are shown in Table 2. Based on Table 2, the dynamic range and LOD of GCE-tPANI-MWCNT-Au@Pt were significantly improved when compared with those reported ones for the electrochemical detection of all six OTC drug molecules.

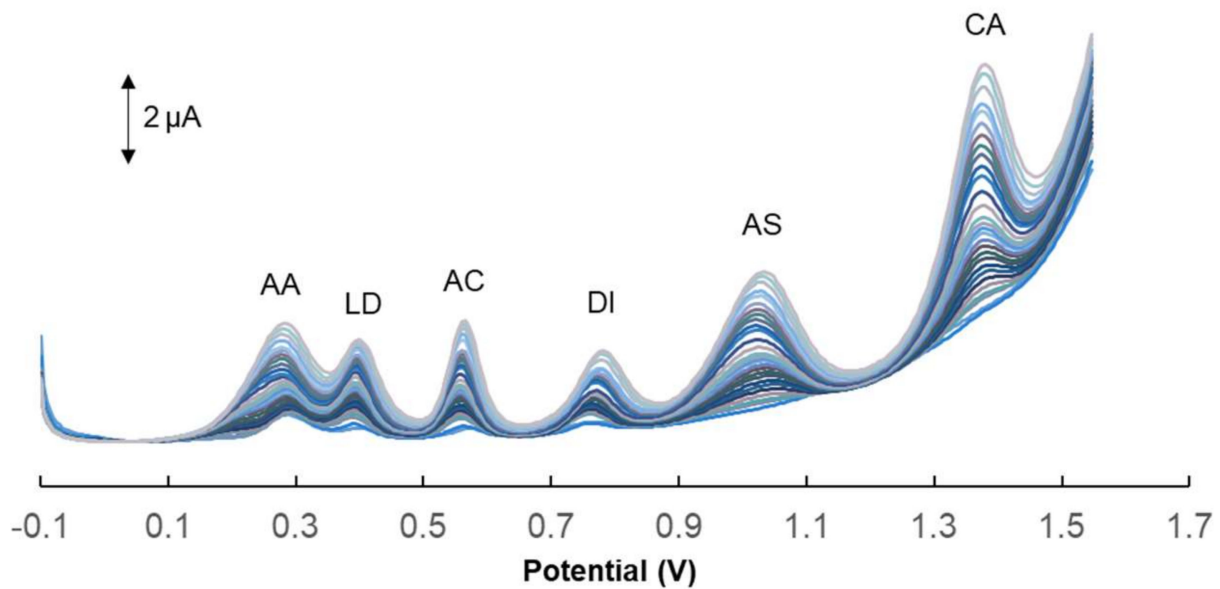


Figure 7. Differential pulse voltammograms for the dependence of oxidation current responses obtained from GCE-tPANI-Au@Pt-MWCNT on the concentration of AA (5.0–570.0 μM), LD (0.5–60.0 μM), AC (0.5–55 μM), DI (0.5–115 μM), AS (5.0–375.0 μM) and CA (5.0–520 μM) in 0.5 M PBS (pH 3.0).

Table 1. Summary of the calibration curves and the R^2 values of the linear fit, the limit of detection (LOD) and the dynamic range for the electrochemical detection of six OTC drug molecules using GCE-tPANI-Au@Pt-MWCNT.

Analyte			LOD (μM)	Dynamic Range (μM)
	I	II		
AA	$\Delta I_{p1} = 0.0053x + 0.5031$ $R^2 = 0.9951$	$\Delta I_{p2} = 0.0035x + 0.7869$ $R^2 = 0.9937$	1.5	5.0–150.0 150.0–570.0
LD	$\Delta I_{p1} = 0.0584[\text{LD}] + 0.4826$ $R^2 = 0.9889$	$\Delta I_{p2} = 0.0195x + 1.249$ $R^2 = 0.9816$	0.25	0.5–20 20–60.0
AC	$\Delta I_{p1} = 0.0545[\text{AC}] + 0.4393$ $R^2 = 0.991$	$\Delta I_{p2} = 0.0307[\text{AC}] + 1.00071$ $R^2 = 0.991$	0.15	0.5–25.0 25.0–60.0
DI	$\Delta I_{p1} = 0.0536[\text{DI}] + 0.4721$ $R^2 = 0.9897$	$\Delta I_{p2} = 0.0093[\text{DI}] + 1.1002$ $R^2 = 0.9922$	0.2	0.5–15.0 15.0–115.0
AS	$\Delta I_p = 0.0066[\text{AS}] + 1.0234$ $R^2 = 0.9912$	-	2.0	5.0–375.0
CA	$\Delta I_{p1} = 0.0101[\text{CA}] + 3.665$ $R^2 = 0.9933$	-	2.5	5.0–520.0

Table 2. Comparison of GCE-tPANI-Au@Pt-MWCNT with the existing electrochemical sensors reported for the detection of ascorbic acid (AA), levodopa (LD), acetaminophen (AC), diclofenac (DI), acetylsalicylic acid (AS) and caffeine (CA) in the literature.

Analyte	Electrode	LOD/ μM	Dynamic Range/ μM	Ref
AA	Au/RGO/GCE ¹	51.0	240.0–1500.0	[9]
	PG/GCE ²	6.45	9.0–2314.0	[40]
	PPF/GNS ³	120.0	400.0–6000.0	[41]
	NG/GCE ⁴	22.0	50.0–1300.0	[42]
	ERGO/GCE ⁵	250.0	500.0–2000.0	[43]
	Pd/CNFs ⁶	15	50.0–4000.0	[44]
	GCE-tPANI-Au@Pt-MWCNT	1.5	5.0–570.0 μM	This study

Table 2. Cont.

Analyte	Electrode	LOD/ μM	Dynamic Range/ μM	Ref
LD	Au screen-printed electrode	0.99	1.0–660.0	[11]
	Modified CP-TNMCPE ⁷	0.069	0.1–100.0	[45]
	GR/ZnO/SPE ⁸	0.45	1.0–1000.0	[46]
	GR/ZnO/SPE	0.09	0.25–200.0	[47]
	CNT paste/EBNBH ⁹	0.094	0.2–700.0	[48]
	GCE-tPANI-Au@Pt-MWCNT	0.25	0.5–60	This study
	NiO/CNTs/DPID/CPEs ¹⁰	0.3	0.8–550.0	[49]
AC	(poly(solochrome black-T)/ GCE	0.14	0.5–50.0	[7]
	GR-CS/GCE ¹¹	0.03	1.0–100.0	[50]
	PANI-MWCNTs modified electrode ¹²	0.25	1.0–100.0	[51]
	SWNT-DCP GCE ¹³	0.04	0.1–20.0	[20]
	NiO-CuO/GR/GCE ¹⁴	1.33	4.0–400.0	[52]
	GCE-tPANI-Au@Pt-MWCNT	0.15	0.5–55.0	This study
	VfMWCNTPE ¹⁵	2.0	5.0–600.0	[53]
DI	CuZEGE electrode ¹⁶	0.05	0.3–20.0	[54]
	BDD electrode ¹⁷	0.03	0.31–31.1	[55]
	NiO-SWCNTs/DDPM/CPE ¹⁸	0.008	0.04–1200.0	[56]
	AuNP/MWCNT/GCE ¹⁹	0.02	0.03–200.0	[6]
	GCE-tPANI-Au@Pt-MWCNT	0.2	0.5–114.0	This study
	MIP film electrochemical sensor ²⁰	0.0003	0.001–0.7	[57]
	Graphene modified GCE	0.02	1–200.0	[58]
AS	ZnO/NP/IL/CPE ²¹	0.3	0.7–950.0	[59]
	SPGrE ²²	0.09	0.1–100.0	[60]
	ISSM-CNT-PE ²³	0.084	0.2–62.0	[38]
	GCE-tPANI-Au@Pt-MWCNT	2.0	5.0–375.0	This study
	Nafion-Gr/GCE ²⁴	0.12	0.4–40.0	[39]
	GNPs/MWCNTs/GCE ²⁵	0.0005	0.0005–0.160	[24]
	MnFe ₂ O ₄ @CNT-N/GCE ²⁶	0.83	1.0–1100.0	[61]
CA	ISSM-CNT-PE	0.08	0.291–62.7	[38]
	GCE-tPANI-Au@Pt-MWCNT	2.5	5.0–520.0	This study

¹ Au/RGO/GCE: Gold/reduced graphene oxide/glassy carbon electrode. ² PG/GCE: Pristine graphene/glassy carbon electrode. ³ PPF/GNS: Pyrolyzed photoresist film/graphene nano-sheets. ⁴ NG/GCE: Nano-gold/glassy carbon electrode. ⁵ ERGO/GCE: Electrochemically reduced graphene oxide/glassy carbon electrode. ⁶ Pd/CNFs: Palladium nanoparticle-loaded carbon nanofibers. ⁷ CP-TNMCPE: Cobalt porphyrin-TiO₂ nanoparticle-modified carbon paste electrode. ⁸ GR/ZnO/SPE: Graphene oxide/zinc oxide nanorods/screen-printed electrode. ⁹ CNT paste/EBNBH: Carbon nanotube paste/ 2,2'-[1,2-ethanediybis (nitriloethylidyne)]-bis-hydroquinone. ¹⁰ NiO/CNTs/DPID/CPEs: Nickel oxide/carbon nanotube/ (2-(3,4-dihydroxyphenethyl) isoindoline-1,3-dione)/carbon paste electrodes. ¹¹ GR-CS/GCE: Graphene chitosan/glassy carbon electrode. ¹² PANI-MWCNTs composite modified electrode: Polyaniline-multi-walled carbon nanotubes. ¹³ SWNT-DCP modified GCE: Singled-wall carbon nanotube-dicetyl phosphate modified glassy carbon electrode. ¹⁴ NiO-CuO/GR/GCE: Nickel oxide-copper oxide nanoparticles-graphene composite film modified glassy carbon electrode. ¹⁵ VfMWCNTPE: Vinylferrocene modified multi-walled carbon nanotubes paste electrode. ¹⁶ CuZEGE electrode: Copper doped zeolite-expanded graphite-epoxy electrode. ¹⁷ BDD electrode: Boron-doped diamond electrode. ¹⁸ NiO-SWCNTs/DDPM/CPE: NiO-SWCNTs as conductive mediator and 2, 4-dimethyl-N-[1-(2, 3-dihydroxy phenyl) methylidene] aniline carbon paste electrode. ¹⁹ AuNP/MWCNT/GCE: Gold nanoparticles/multi-walled carbon nanotube/glassy carbon electrode. ²⁰ MIP: Molecular imprinted polymer. ²¹ ZnO/NP/IL/CPE: Zinc oxide nanoparticles ionic liquid carbon paste electrode. ²² SPGrE: Screen-printed graphene electrode. ²³ ISSM-CNT-PE: In-situ surfactant-modified multi-walled carbon nanotube paste electrode. ²⁴ Nafion-Gr/GCE: Nafion-graphene/glassy carbon electrode. ²⁵ GNPs/MWCNTs/GCE: Gold nanoparticles/multi-walled carbon nanotubes/glassy carbon electrode. ²⁶ MnFe₂O₄@CNT-N/GCE: N-doped carbon nanotubes functionalized with MnFe₂O₄ magnetic nanoparticles functionalized glassy carbon electrode.

3.6. Chronoamperometry

In order to understand the electrochemical reaction under diffusive mass-transport limitation, the diffusion coefficients (D) of AA, LD, AC, DI, AS and CA were determined using chronoamperometry. The measurements were performed in 0.5 M PBS buffer (pH 3.0) over a period of 10 s at a constant applied potential of 0.289, 0.408, 0.571, 0.786, 1.027, and 1.380 V which were assigned as the anodic peak potential of AA, LD, AC, DI, AS and CA, respectively, from our DPV studies. As an example, the determination of D of AC was determined as shown in Figure 8. A plot of I vs. $t^{-1/2}$ was generated, and the linear region was fitted through a linear line of best-fit to obtain the slope (Figure 8b). Finally, the slopes

were plotted against the concentration of AC spiked in the measurement cell (Figure 8c). The Cottrell relation was applied:

$$i = nFACD^{1/2}(\pi t)^{-1/2} \quad (7)$$

where i is the current (A), n is the number of electrons exchanged, F is the Faraday's constant (96,485 C/mol), A is the area of the working electrode (determined to be 0.071 cm²), C is the concentration analyte in the bulk solution, D is the diffusion coefficient (cm².s⁻¹), and t is time (s). The same set of chronoamperometric studies were performed for each of the six drug molecules. The calculated values of D were 2.0181×10^{-6} , 3.2857×10^{-5} , 3.5822×10^{-6} , 2.2832×10^{-6} , 6.5608×10^{-7} , and 4.1989×10^{-7} cm². s⁻¹ for AA, LD, AC, DI, AS and CA, respectively. In our preliminary results, it was found that the magnitudes of the calculated diffusion coefficients were comparable to those reported in the literature. Further experimental work is under progress in our laboratory to achieve more conclusive results to determine the diffusion coefficients (Table 3).

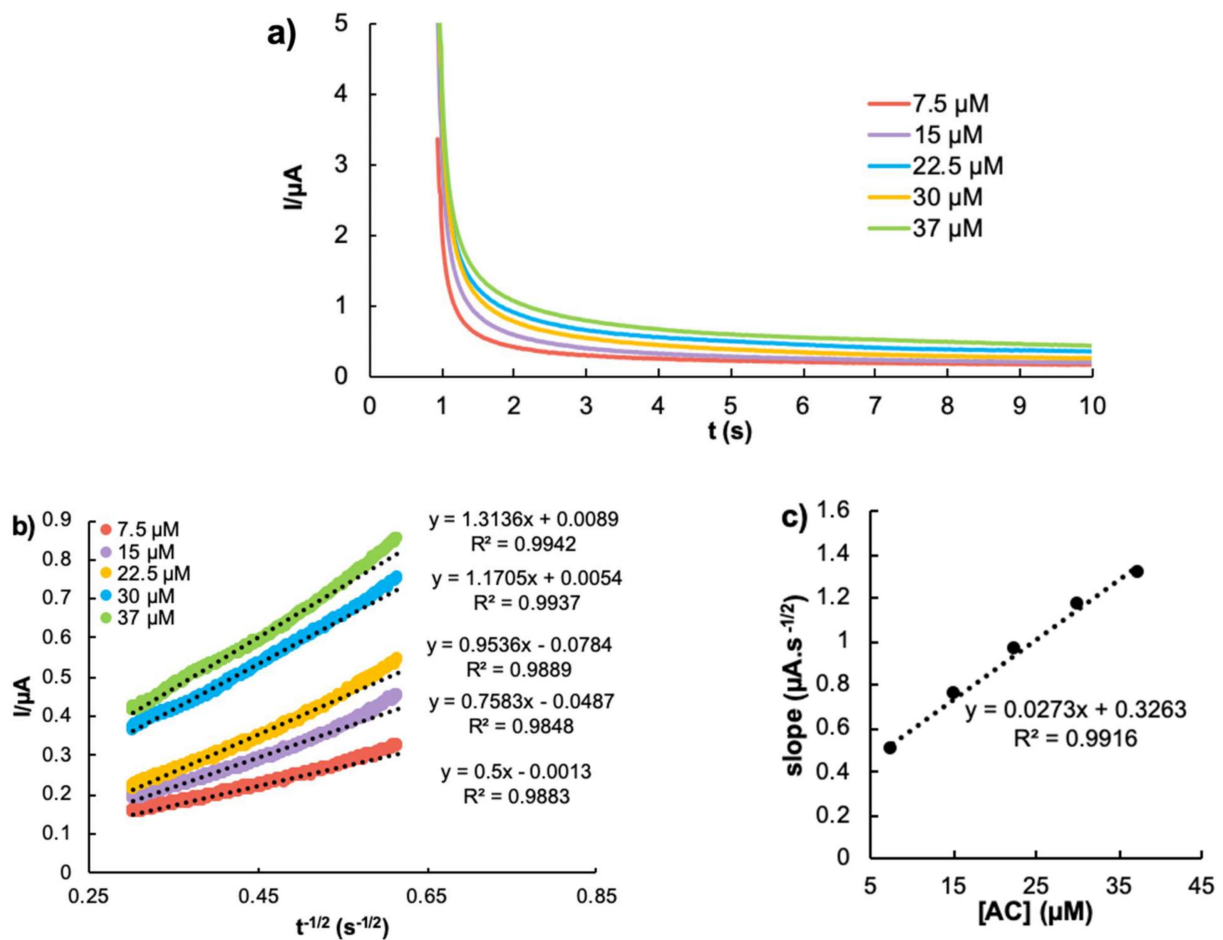


Figure 8. (a) Chronoamperograms of tPANI-Au@Pt-MWCNT-GCE in the presence of increasing concentrations of AC; 7.5 μM (red), 15 μM (purple), 22.5 μM (blue), 30 μM (yellow), and 37 μM (green) in 0.5 M PBS (pH 3.0), (b) the $t^{-1/2}$ vs. I_{pa} plots, and (c) is the slope obtained from (b) plotted against the concentration of AC.

Table 3. Summary of the calculated diffusion coefficients (D) and the comparison to previously reported values using various modified electrodes.

Analyte	Diffusion Coefficient ($\text{cm}^2 \text{s}^{-1}$)	Reference
AA	1.87×10^{-5}	[62]
	4.0×10^{-6}	[63]
	9.07×10^{-6}	[64]
	1.33×10^{-6}	[65]
	2.02×10^{-6}	This work
LD	2.09×10^{-4}	[66]
	1.9×10^{-6}	[67]
	1.06×10^{-6}	[68]
	6.70×10^{-6}	[69]
	3.29×10^{-5}	This work
AC	1.25×10^{-5}	[38]
	4.97×10^{-6}	[65]
	5.91×10^{-6}	[51]
	1.09×10^{-9}	[50]
	3.58×10^{-6}	This work
DI	3.39×10^{-4}	[67]
	5.9×10^{-6}	[70]
	2.67×10^{-6}	[71]
	3.7×10^{-4}	[53]
	2.28×10^{-6}	This work
AS	1.536×10^{-5}	[38]
	6.46×10^{-6}	[72]
	7.1×10^{-6}	[10]
	7.84×10^{-6}	[73]
	6.56×10^{-7}	This work
CA	2.174×10^{-5}	[74]
	5.236×10^{-6}	[75]
	4.2×10^{-5}	[75]
	1.095×10^{-5}	[38]
	4.1989×10^{-7}	This work

3.7. Sensor Reproducibility, Stability, and Interference

To demonstrate that GCE-tPANI-Au@Pt-MWCNT provided stable and reproducible results, ten independent measurements in the presence of AA (100 μM) LD (25 μM), AC (25 μM), DI (50 μM), AS (150 μM) and CA (150 μM) were performed. As shown in Figure S6a–c, the current peaks for AA, LD, AC, DI, AS and CA demonstrated a relative standard deviation of peak height at the same potential of 0.62%, 0.27%, 0.63%, 0.44%, 0.28% and 0.33%, respectively ($n = 10$). Next, to demonstrate the GCE-PANI-Au@Pt-MWCNT sensor is stable over time, AA (100 μM) LD (25 μM), AC (25 μM), DI (50 μM), AS (150 μM) and CA (150 μM) were measured over a period of 45 days (Figure S6d). The signal retention was 95.3%, 95.2%, 104.1%, 97.79%, 95.70%, and 97.06% for AA, LD, AC, DI, AS and CA, respectively, suggesting the electrodes were stable. Finally, interference study was performed to show that the OTC drug molecules did not interfere with each other during electrochemical detection. As shown in the differential pulse voltammograms of Figure S7, five drug molecules were kept at a fixed concentration while the concentration of one of the chosen molecules were increased. Each drug molecule demonstrated a linear response with the following equations for AA: $I_{\text{pa}} = 0.0028 [\text{AA}] + 0.8202$ ($R^2 = 0.9905$), LD: $I_{\text{pa}} = 0.0457[\text{LD}] + 1.0606$ ($R^2 = 0.9943$), AC: $I_{\text{pa}} = 0.0628[\text{AC}] + 0.3714$ ($R^2 = 0.9856$), DI: $I_{\text{pa}} = 0.0312[\text{DI}] + 0.5019$ ($R^2 = 0.9822$), AS: $I_{\text{pa}} = 0.0089[\text{AS}] + 0.7102$ ($R^2 = 0.9812$) and CA: $I_{\text{pa}} = 0.0102[\text{DI}] + 2.9973$ ($R^2 = 0.9991$).

3.8. Real Sample Analyses in Commercial Products

To determine the applicability of the GCE-tPANI-Au@Pt-MWCNT sensor in real samples, commercially available pharmaceutical products such as tablets and cream were purchased and analyzed for their contents containing the six chosen molecules. For this purpose, five OTC drug molecules were purchased from commercial sources and diluted using distilled water as described in the Materials and Methods 2.6 section. The results for individual determinations of AA, AC, DI AS, and within the selected commercial products are summarized in Table 4. The “Detected” is the analyte concentration found, as reported by their nutrition label on the products. The “Determined” is the analyte concentration that was detected after correlating the signal obtained from the sensor through a standard addition method ($n = 5$). Recovery percentage was calculated by dividing “determined” by “detected” and multiplying by 100%. The results showed that the recovery percentages ranged between 95.5 ± 0.53 and $104.1 \pm 1.63\%$, suggesting that the sensor platform can detect the targeted molecules in the samples purchased from commercial sources.

Table 4. Application of GCE-tPANI-Au@Pt-MWCNT for individual determinations of AA, AC, DI, AS and CA in the commercial products ($n = 4$, for the reported relative standard deviation (RSD) values).

	Analyte	Detected (μM)	Determined (μM)	Recovery (%)
Vitamin Water™ (Energy drink)	AA	70	68.08 ± 13.04	98.2 ± 1.89
Pseudoephedrine Hydrochloride (Tablet)	AC	52.9	51.84 ± 4.67	97.95 ± 2.42
Voltaren™ (Cream)	DI	5.54	5.37 ± 0.42	96.9 ± 3.52
Aspirin™ (Tablet)	AS	111	105.21 ± 6.52	95.48 ± 0.53
Caffeine Tablet	CA	205.67	214.28 ± 10.42	104.1 ± 1.63

4. Conclusions

Herein, a novel nanocomposite was synthesized for the construction of a sensor to detect six redox-active drug molecules simultaneously for the first time, to the best of our knowledge. This nanocomposite, tPANI-Au@Pt-MWCNT, was characterized using FT-IR, TEM, and XPS to demonstrate the successful synthesis. The incorporation of tPANI-Au@Pt-MWCNT to the GCEs provided an enhanced electrocatalytic activity as reflected by CV and EIS. The sensor allowed the sensitive determination of all six OTC drug molecules in one measurement using DPV. Moreover, the sensor demonstrated good reproducibility and stability over a period of 45 days of storage time, as well as acceptable recovery values when determined in commercially available OTC products. In connection with the optimized sampling and chromatographic separation systems, we envisage that this electrochemical sensor GCE-tPANI-Au@Pt-MWCNT can become a powerful tool for the sensitive determination of redox-active drug molecules in toxicological and forensic investigations. The pharmacokinetic properties of the therapeutic drugs can also be determined in real samples upon adjusting the pH and ionic strength to the optimized conditions reported here. The electrochemical sensors can be miniaturized for easy on-site applications to allow law enforcement agents to detect the abuse of drugs. With the exponential growth of nanomaterials, the nanocomposite-modified electrochemical sensors and biosensors are poised to appear in the market in the near future.

Supplementary Materials: The XPS survey spectra of nanomaterial-modified surfaces, DPV studies for the pH dependence of current responses, calibration plots, repeatability, stability and interference studies are available online at <https://www.mdpi.com/2227-9040/9/2/24/s1>.

Author Contributions: S.L., J.Z., M.N. and K.K. conceived the experimental plan. S.L., J.Z., M.N. performed all experiments. S.L., J.Z., M.N. and K.K. analyzed the data. S.L., J.Z., M.N. and K.K. wrote the manuscript. All authors have given approval to the final version of the manuscript.

Funding: K.K. acknowledges financial support from the Canada Research Chairs Tier-2 award for “Bioelectrochemistry of Proteins” (Project no.950-231116), Ontario Ministry of Research, Innovation and Science (Project no. 35272), Discovery Grant (Project no. 3655) from NSERC Canadian Network for Research and Innovation in Machining Technology, and Canada Foundation for Innovation (Project no. 35272).

Institutional Review Board Statement: Not applicable.

Informed Consent Statement: Not applicable.

Data Availability Statement: The data presented in this study are available on request from the corresponding author. The data are not publicly available due to pending patent applications.

Acknowledgments: S.L. gratefully acknowledges Ontario Graduate Scholarship (OGS). K.K. acknowledges Canada Research Chair Tier-2 award (project no. 950-231116), the Ontario Ministry of Research, Innovation and Science (Project no. 35272), Discovery Grant (project no. 3655) from the Natural Sciences and Engineering Research Council of Canada (NSERC), and the Canada Foundation for Innovation (project no. 35272).

Conflicts of Interest: The authors declare no conflict of interest.

References

1. Gurpinar, E.; Grizzle, W.E.; Piazza, G.A. NSAIDs inhibit tumorigenesis, but how? *Clin. Cancer Res.* **2014**, *20*, 1104–1113. [[CrossRef](#)] [[PubMed](#)]
2. Da Mata, A.M.O.F.; De Carvalho, R.M.; De Alencar, M.V.O.B.; De Carvalho Melo Cavalcante, A.A.; Da Silva, B.B. Ascorbic acid in the prevention and treatment of cancer. *Rev. Assoc. Med. Bras.* **2016**, *62*, 680–686. [[CrossRef](#)] [[PubMed](#)]
3. Băjenaru, O.; Ene, A.; Popescu, B.O.; Szász, J.A.; Sabău, M.; Mureșan, D.F.; Perju-Dumbrava, L.; Popescu, C.D.; Constantinescu, A.; Buraga, I.; et al. The effect of levodopa–carbidopa intestinal gel infusion long-term therapy on motor complications in advanced Parkinson’s disease: A multicenter Romanian experience. *J. Neural Transm.* **2016**, *123*, 407–414. [[CrossRef](#)]
4. Medve, R.A.; Wang, J.; Karim, R. Tramadol and acetaminophen tablets for dental pain. *Anesth. Prog.* **2001**, *48*, 79–81.
5. Diamond, S.; Balm, T.K.; Freitag, F.G. Ibuprofen plus caffeine in the treatment of tension-type headache. *Clin. Pharmacol. Ther.* **2000**, *68*, 312–319. [[CrossRef](#)]
6. Afkhami, A.; Bahiraei, A.; Madrakian, T. Gold nanoparticle/multi-walled carbon nanotube modified glassy carbon electrode as a sensitive voltammetric sensor for the determination of diclofenac sodium. *Mater. Sci. Eng. C* **2016**, *59*, 168–176. [[CrossRef](#)]
7. Daneshinejad, H.; Chamjangali, M.A.; Goudarzi, N.; Roudbari, A. Application of a thin film of poly(solochrome black T) as a redox mediator for the electro-catalytic simultaneous determination of dopamine and acetaminophen in the pharmaceutical and biological samples. *Mater. Sci. Eng. C* **2016**, *58*, 532–540. [[CrossRef](#)] [[PubMed](#)]
8. Teymourian, H.; Parrilla, M.; Sempionatto, J.R.; Montiel, N.F.; Barfidokht, A.; Van Echelpoel, R.; De Wael, K.; Wang, J. Wearable Electrochemical Sensors for the Monitoring and Screening of Drugs. *ACS Sens.* **2020**, *5*, 2679–2700. [[CrossRef](#)]
9. Wang, C.; Du, J.; Wang, H.; Zou, C.; Jiang, F.; Yang, P.; Du, Y. A facile electrochemical sensor based on reduced graphene oxide and Au nanoplates modified glassy carbon electrode for simultaneous detection of ascorbic acid, dopamine and uric acid. *Sens. Actuators B Chem.* **2014**, *204*, 302–309. [[CrossRef](#)]
10. Wudarska, E.; Chrzescijanska, E.; Kusmierk, E.; Rynkowski, J. Voltammetric studies of acetylsalicylic acid electrooxidation at platinum electrode. *Electrochim. Acta* **2013**, *93*, 189–194. [[CrossRef](#)]
11. Bergamini, M.F.; Santos, A.L.; Stradiotto, N.R.; Zanoni, M.V.B. A disposable electrochemical sensor for the rapid determination of levodopa. *J. Pharm. Biomed. Anal.* **2005**, *39*, 54–59. [[CrossRef](#)]
12. Serrano, N.; Castilla, Ò.; Ariño, C.; Diaz-Cruz, M.S.; Díaz-Cruz, J.M. Commercial screen-printed electrodes based on carbon nanomaterials for a fast and cost-effective voltammetric determination of paracetamol, ibuprofen and caffeine in water samples. *Sensors* **2019**, *19*, 4039. [[CrossRef](#)] [[PubMed](#)]
13. Yu, M.F.; Lourie, O.; Dyer, M.J.; Moloni, K.; Kelly, T.F.; Ruoff, R.S. Strength and breaking mechanism of multiwalled carbon nanotubes under tensile load. *Science* **2000**, *287*, 637–640. [[CrossRef](#)] [[PubMed](#)]
14. Catalysis, R.S.C.; No, S.; Materials, N.C.; By, C.; Serp, P.; Machado, B.; Serp, P.; Machado, B. *Nanostructured Carbon Materials for Catalysis*; Royal Society of Chemistry: London, UK, 2015; ISBN 9781782622567.
15. Taylor, R.L. American association for the advancement of science. *J. Clin. Endocrinol. Metab.* **1950**, *10*, 1361–1362.
16. Chung, D.D.L. Review: Graphite. *J. Mater. Sci.* **2002**, *37*, 1475–1489. [[CrossRef](#)]
17. Saifuddin, N.; Raziah, A.Z.; Junizah, A.R. Carbon nanotubes: A review on structure and their interaction with proteins. *J. Chem.* **2013**, *2013*, 676815. [[CrossRef](#)]
18. Alsharif, J.M.A.; Taha, M.R.; Khan, T.A. Physical dispersion of nanocarbons in composites—A review. *J. Teknol.* **2017**, *79*, 69–81. [[CrossRef](#)]
19. Spitalsky, Z.; Tasis, D.; Papagelis, K.; Galiotis, C. Carbon nanotube-polymer composites: Chemistry, processing, mechanical and electrical properties. *Prog. Polym. Sci.* **2010**, *35*, 357–401. [[CrossRef](#)]

20. Sun, D.; Zhang, H. Electrochemical determination of acetaminophen using a glassy carbon electrode coated with a single-wall carbon nanotube-dicetyl phosphate film. *Microchim. Acta* **2007**, *158*, 131–136. [[CrossRef](#)]
21. Chakraborty, I.; Chakrabarty, N.; Senapati, A.; Chakraborty, A.K. CuO@NiO/Polyaniline/MWCNT Nanocomposite as High-Performance Electrode for Supercapacitor. *J. Phys. Chem. C* **2018**, *122*, 27180–27190. [[CrossRef](#)]
22. Abdulla, S.; Mathew, T.L.; Pullithadathil, B. Highly sensitive, room temperature gas sensor based on polyaniline-multiwalled carbon nanotubes (PANI/MWCNTs) nanocomposite for trace-level ammonia detection. *Sens. Actuators B Chem.* **2015**, *221*, 1523–1534. [[CrossRef](#)]
23. Afkhami, A.; Soltani-Felehgari, F.; Madrakian, T. A sensitive electrochemical sensor for rapid determination of methadone in biological fluids using carbon paste electrode modified with gold nanofilm. *Talanta* **2014**, *128*, 203–210. [[CrossRef](#)] [[PubMed](#)]
24. Kan, X.; Liu, T.; Li, C.; Zhou, H.; Xing, Z.; Zhu, A. A novel electrochemical sensor based on molecularly imprinted polymers for caffeine recognition and detection. *J. Solid State Electrochem.* **2012**, *16*, 3207–3213. [[CrossRef](#)]
25. Yang, M.; Yang, Y.; Liu, Y.; Shen, G.; Yu, R. Platinum nanoparticles-doped sol-gel/carbon nanotubes composite electrochemical sensors and biosensors. *Biosens. Bioelectron.* **2006**, *21*, 1125–1131. [[CrossRef](#)]
26. Hrapovic, S.; Liu, Y.; Male, K.B.; Luong, J.H.T. Electrochemical Biosensing Platforms Using Platinum Nanoparticles and Carbon Nanotubes. *Anal. Chem.* **2004**, *76*, 1083–1088. [[CrossRef](#)]
27. Gautam, V.; Singh, K.P.; Yadav, V.L. Polyaniline/MWCNTs/starch modified carbon paste electrode for non-enzymatic detection of cholesterol: Application to real sample (cow milk). *Anal. Bioanal. Chem.* **2018**, *410*, 2173–2181. [[CrossRef](#)]
28. Li, S.; Noroozifar, M.; Kerman, K. Nanocomposite of ferricyanide-doped chitosan with multi-walled carbon nanotubes for simultaneous sensory detection of redox-active biomolecules. *J. Electroanal. Chem.* **2019**, *849*, 113376. [[CrossRef](#)]
29. Zhou, J.; Li, S.; Noroozifar, M.; Kerman, K. Graphene oxide nanoribbons in chitosan for simultaneous electrochemical detection of guanine, adenine, thymine and cytosine. *Biosensors* **2020**, *10*, 30. [[CrossRef](#)]
30. Patel, B.R.; Imran, S.; Ye, W.; Weng, H.; Noroozifar, M.; Kerman, K. Simultaneous voltammetric detection of six biomolecules using a nanocomposite of titanium dioxide nanorods with multi-walled carbon nanotubes. *Electrochim. Acta* **2020**, *362*, 137094. [[CrossRef](#)]
31. Turkevich, J.; Stevenson, P.C.; Hillier, J. A study of the nucleation and growth processes in the synthesis of colloidal gold. *Discuss. Faraday Soc.* **1951**, *11*, 55–75. [[CrossRef](#)]
32. Tan, C.; Sun, Y.; Zheng, J.; Wang, D.; Li, Z.; Zeng, H.; Guo, J.; Jing, L.; Jiang, L. A self-supporting bimetallic Au@Pt core-shell nanoparticle electrocatalyst for the synergistic enhancement of methanol oxidation. *Sci. Rep.* **2017**, *7*, 1–10. [[CrossRef](#)] [[PubMed](#)]
33. Rosario-Castro, B.I.; Fachini, E.R.; Hernández, J.; Pérez-Davis, M.E.; Cabrera, C.R. Electrochemical and surface characterization of 4-aminothiophenol adsorption at polycrystalline platinum electrodes. *Langmuir* **2006**, *22*, 6102–6108. [[CrossRef](#)] [[PubMed](#)]
34. Patil, S.H.; Gaikwad, A.P.; Sathaye, S.D.; Patil, K.R. To form layer by layer composite film in view of its application as supercapacitor electrode by exploiting the techniques of thin films formation just around the corner. *Electrochim. Acta* **2018**, *265*, 556–568. [[CrossRef](#)]
35. Okpalugo, T.I.T.; Papakonstantinou, P.; Murphy, H.; McLaughlin, J.; Brown, N.M.D. High resolution XPS characterization of chemical functionalised MWCNTs and SWCNTs. *Carbon N. Y.* **2005**, *43*, 153–161. [[CrossRef](#)]
36. Gowthaman, N.S.K.; John, S.A. Modification of a glassy carbon electrode with gold-platinum core-shell nanoparticles by electroless deposition and their electrocatalytic activity. *RSC Adv.* **2015**, *5*, 42369–42375. [[CrossRef](#)]
37. Song, E.; Choi, J.-W. Conducting Polyaniline Nanowire and Its Applications in Chemiresistive Sensing. *Nanomaterials* **2013**, *3*, 498–523. [[CrossRef](#)]
38. Sanghavi, B.J.; Srivastava, A.K. Simultaneous voltammetric determination of acetaminophen, aspirin and caffeine using an in situ surfactant-modified multiwalled carbon nanotube paste electrode. *Electrochim. Acta* **2010**, *55*, 8638–8648. [[CrossRef](#)]
39. Sun, J.Y.; Huang, K.J.; Wei, S.Y.; Wu, Z.W.; Ren, F.P. A graphene-based electrochemical sensor for sensitive determination of caffeine. *Colloids Surf. B Biointerfaces* **2011**, *84*, 421–426. [[CrossRef](#)]
40. Qi, S.; Zhao, B.; Tang, H.; Jiang, X. Determination of ascorbic acid, dopamine, and uric acid by a novel electrochemical sensor based on pristine graphene. *Electrochim. Acta* **2015**, *161*, 395–402. [[CrossRef](#)]
41. Keeley, G.P.; O'Neill, A.; McEvoy, N.; Peltekis, N.; Coleman, J.N.; Duesberg, G.S. Electrochemical ascorbic acid sensor based on DMF-exfoliated graphene. *J. Mater. Chem.* **2010**, *20*, 7864–7869. [[CrossRef](#)]
42. Hosseini, H.; Behbahani, M.; Mahyari, M.; Kazerooni, H.; Bagheri, A.; Shaabani, A. Ordered carbohydrate-derived porous carbons immobilized gold nanoparticles as a new electrode material for electrocatalytic oxidation and determination of nicotinamide adenine dinucleotide. *Biosens. Bioelectron.* **2014**, *59*, 412–417. [[CrossRef](#)] [[PubMed](#)]
43. Yang, L.; Liu, D.; Huang, J.; You, T. Simultaneous determination of dopamine, ascorbic acid and uric acid at electrochemically reduced graphene oxide modified electrode. *Sens. Actuators B Chem.* **2014**, *193*, 166–172. [[CrossRef](#)]
44. Huang, J.; Liu, Y.; Hou, H.; You, T. Simultaneous electrochemical determination of dopamine, uric acid and ascorbic acid using palladium nanoparticle-loaded carbon nanofibers modified electrode. *Biosens. Bioelectron.* **2008**, *24*, 632–637. [[CrossRef](#)] [[PubMed](#)]
45. Mazloum-Ardakani, M.; Taleat, Z.; Khoshroo, A.; Beitollahi, H.; Dehghani, H. Electrocatalytic oxidation and voltammetric determination of levodopa in the presence of carbidopa at the surface of a nanostructure based electrochemical sensor. *Biosens. Bioelectron.* **2012**, *35*, 75–81. [[CrossRef](#)]
46. Beitollahi, H.; Nejad, F.G. Graphene Oxide/ZnO Nano Composite for Sensitive and Selective Electrochemical Sensing of Levodopa and Tyrosine Using Modified Graphite Screen Printed Electrode. *Electroanalysis* **2016**, *28*, 2237–2244. [[CrossRef](#)]

47. Beitollahi, H.; Mostafavi, M. Nanostructured base electrochemical sensor for simultaneous quantification and voltammetric studies of levodopa and carbidopa in pharmaceutical products and biological samples. *Electroanalysis* **2014**, *26*, 1090–1098. [[CrossRef](#)]
48. Mazloum-Ardakani, M.; Ganjipour, B.; Beitollahi, H.; Amini, M.K.; Mirkhalaf, F.; Naeimi, H.; Nejati-Barzoki, M. Simultaneous determination of levodopa, carbidopa and tryptophan using nanostructured electrochemical sensor based on novel hydroquinone and carbon nanotubes: Application to the analysis of some real samples. *Electrochim. Acta* **2011**, *56*, 9113–9120. [[CrossRef](#)]
49. Karimi-Maleh, H.; Ganjali, M.R.; Norouzi, P.; Bananezhad, A. Amplified nanostructure electrochemical sensor for simultaneous determination of captopril, acetaminophen, tyrosine and hydrochlorothiazide. *Mater. Sci. Eng. C* **2017**, *73*, 472–477. [[CrossRef](#)]
50. Zheng, M.; Gao, F.; Wang, Q.; Cai, X.; Jiang, S.; Huang, L.; Gao, F. Electrocatalytic oxidation and sensitive determination of acetaminophen on glassy carbon electrode modified with graphene-chitosan composite. *Mater. Sci. Eng. C* **2013**, *33*, 1514–1520. [[CrossRef](#)]
51. Li, M.; Jing, L. Electrochemical behavior of acetaminophen and its detection on the PANI-MWCNTs composite modified electrode. *Electrochim. Acta* **2007**, *52*, 3250–3257. [[CrossRef](#)]
52. Liu, B.; Ouyang, X.; Ding, Y.; Luo, L.; Xu, D.; Ning, Y. Electrochemical preparation of nickel and copper oxides-decorated graphene composite for simultaneous determination of dopamine, acetaminophen and tryptophan. *Talanta* **2016**, *146*, 114–121. [[CrossRef](#)]
53. Mokhtari, A.; Karimi-Maleh, H.; Ensafi, A.A.; Beitollahi, H. Application of modified multiwall carbon nanotubes paste electrode for simultaneous voltammetric determination of morphine and diclofenac in biological and pharmaceutical samples. *Sens. Actuators B Chem.* **2012**, *169*, 96–105. [[CrossRef](#)]
54. Manea, F.; Ihos, M.; Remes, A.; Burtica, G.; Schoonman, J. Electrochemical determination of diclofenac sodium in aqueous solution on Cu-Doped zeolite-expanded graphite-epoxy electrode. *Electroanalysis* **2010**, *22*, 2058–2063. [[CrossRef](#)]
55. Ihos, M.; Remes, A.; Manea, F. Electrochemical determination of diclofenac using boron-doped diamond electrode. *J. Environ. Prot. Ecol.* **2012**, *13*, 2096–2103.
56. Akbarian, Y.; Shabani-Nooshabadi, M.; Karimi-Maleh, H. Fabrication of a new electrocatalytic sensor for determination of diclofenac, morphine and mefenamic acid using synergic effect of NiO-SWCNT and 2,4-dimethyl-N-[1-(2,3-dihydroxy phenyl) methylidene] aniline. *Sens. Actuators B Chem.* **2018**, *273*, 228–233. [[CrossRef](#)]
57. Wang, Z.; Li, H.; Chen, J.; Xue, Z.; Wu, B.; Lu, X. Acetylsalicylic acid electrochemical sensor based on PATP-AuNPs modified molecularly imprinted polymer film. *Talanta* **2011**, *85*, 1672–1679. [[CrossRef](#)]
58. Patil, S.M.; Sataraddi, S.R.; Bagoji, A.M.; Pathan, R.M.; Nandibewoor, S.T. Electrochemical behavior of graphene-based sensors on the redox mechanism of aspirin. *Electroanalysis* **2014**, *26*, 831–839. [[CrossRef](#)]
59. Karimi-Maleh, H.; Rostami, S.; Gupta, V.K.; Fouladgar, M. Evaluation of ZnO nanoparticle ionic liquid composite as a voltammetric sensing of isoprenaline in the presence of aspirin for liquid phase determination. *J. Mol. Liq.* **2015**, *201*, 102–107. [[CrossRef](#)]
60. Kruanetr, S.; Prabhu, R.; Pollard, P.; Fernandez, C. Pharmaceutical electrochemistry: The electrochemical detection of aspirin utilising screen printed graphene electrodes as sensors platforms. *Surf. Eng. Appl. Electrochem.* **2015**, *51*, 283–289. [[CrossRef](#)]
61. Fernandes, D.M.; Silva, N.; Pereira, C.; Moura, C.; Magalhães, J.M.C.S.; Bachiller-Baeza, B.; Rodríguez-Ramos, I.; Guerrero-Ruiz, A.; Delerue-Matos, C.; Freire, C. MnFe₂O₄@CNT-N as novel electrochemical nanosensor for determination of caffeine, acetaminophen and ascorbic acid. *Sens. Actuators B Chem.* **2015**, *218*, 128–136. [[CrossRef](#)]
62. Han, X.; Tang, J.; Wang, J.; Wang, E. Electrocatalytic oxidation of ascorbic acid by norepinephrine embedded in lipid cast film at glassy carbon electrode. *Electrochim. Acta* **2001**, *46*, 3367–3371. [[CrossRef](#)]
63. Moreno, G.; Pariente, F.; Lorenzo, E. Electrocatalytic oxidation of ascorbate at glassy carbon electrodes modified with electrodeposited films derived from dihydroxybenzaldehyde isomers. *Anal. Chim. Acta* **2000**, *420*, 29–37. [[CrossRef](#)]
64. Zare, H.R.; Nasirizadeh, N.; Ardakani, M.M. Electrochemical properties of a tetrabromo-p-benzoquinone modified carbon paste electrode. Application to the simultaneous determination of ascorbic acid, dopamine and uric acid. *J. Electroanal. Chem.* **2005**, *577*, 25–33. [[CrossRef](#)]
65. Wang, S.F.; Xie, F.; Hu, R.F. Carbon-coated nickel magnetic nanoparticles modified electrodes as a sensor for determination of acetaminophen. *Sens. Actuators B Chem.* **2007**, *123*, 495–500. [[CrossRef](#)]
66. Sivanesan, A.; John, S.A. Determination of L-dopa using electropolymerized 3,3',3'',3'''-tetraaminophthalocyanatonickel(II) film on glassy carbon electrode. *Biosens. Bioelectron.* **2007**, *23*, 708–713. [[CrossRef](#)] [[PubMed](#)]
67. Arvand, M.; Gholizadeh, T.M.; Zanjanchi, M.A. MWCNTs/Cu(OH)₂ nanoparticles/IL nanocomposite modified glassy carbon electrode as a voltammetric sensor for determination of the non-steroidal anti-inflammatory drug diclofenac. *Mater. Sci. Eng. C* **2012**, *32*, 1682–1689. [[CrossRef](#)]
68. Yan, X.X.; Pang, D.W.; Lu, Z.X.; Lü, J.Q.; Tong, H. Electrochemical behavior of L-dopa at single-wall carbon nanotube-modified glassy carbon electrodes. *J. Electroanal. Chem.* **2004**, *569*, 47–52. [[CrossRef](#)]
69. Yan, X.; Pan, D.; Wang, H.; Bo, X.; Guo, L. Electrochemical determination of L-dopa at cobalt hexacyanoferrate/large-mesopore carbon composite modified electrode. *J. Electroanal. Chem.* **2011**, *663*, 36–42. [[CrossRef](#)]
70. Goodarzi, M.; Khalilzade, M.A.; Karimi, F.; Gupta, V.K.; Keyvanfard, M.; Bagheri, H.; Fouladgar, M. Square wave voltammetric determination of diclofenac in liquid phase using a novel ionic liquid multiwall carbon nanotubes paste electrode. *J. Mol. Liq.* **2014**, *197*, 114–119. [[CrossRef](#)]

71. Parvizi-Fard, G.; Alipour, E.; Sefidi, P.Y.; Sabzi, R.E. Pretreated Pencil Graphite Electrode as a Versatile Platform for Easy Measurement of Diclofenac Sodium in a Number of Biological and Pharmaceutical Samples. *J. Chin. Chem. Soc.* **2018**, *65*, 472–484. [[CrossRef](#)]
72. Zavar, M.H.A.; Heydari, S.; Rounaghi, G.H. Electrochemical Determination of Salicylic Acid at a New Biosensor Based on Polypyrrole-Banana Tissue Composite. *Arab. J. Sci. Eng.* **2013**, *38*, 29–36. [[CrossRef](#)]
73. Chrzescijanska, E.; Wudarska, E.; Kusmierk, E.; Rynkowski, J. Study of acetylsalicylic acid electroreduction behavior at platinum electrode. *J. Electroanal. Chem.* **2014**, *713*, 17–21. [[CrossRef](#)]
74. Jesny, S.; Kumar, K.G. Non-enzymatic Electrochemical Sensor for the Simultaneous Determination of Xanthine, Its Methyl Derivatives Theophylline and Caffeine as well as Its Metabolite Uric Acid. *Electroanalysis* **2017**, *29*, 1828–1837. [[CrossRef](#)]
75. Shehata, M.; Azab, S.M.; Fekry, A.M. May glutathione and graphene oxide enhance the electrochemical detection of caffeine on carbon paste sensor in aqueous and surfactant media for beverages analysis? *Synth. Met.* **2019**, *256*, 116122. [[CrossRef](#)]